MVIRT, A TOOLBOX FOR MANIFOLD-VALUED IMAGE RESTORATION

Ronny Bergmann

University of Kaiserslautern, Department of Mathematics
Postbox 3049, D-67653 Kaiserslautern, Germany

ABSTRACT

In many real life application measured data takes its values on Riemannian manifolds. For the special case of the Euclidean space this setting includes the classical grayscale and color images. Like these classical images, manifold-valued data might suffer from measurement errors in form of noise or missing data. In this paper we present the manifold-valued image restoration toolbox (MVIRT) that provides implementations of classical image processing tasks. Based on recent developments in variational methods for manifold-valued image processing methods, like total variation regularization, the toolbox provides easy access to work with these algorithms. The toolbox is implemented in Matlab, open source, and easily extendible, e.g. with own manifolds, noise models or further algorithms. This paper introduces the main mathematical methods as well as numerical examples.

Index Terms— Riemannian manifold, variational models, cyclic proximal point, half-quadratic minimization, Douglas–Rachford splitting

1. INTRODUCTION

In many scenarios, in many applications, measured data might occur not as the usual gray-valued or color image but as data on a Riemannian manifold. For example, when looking at Interferometric Synthetic Aperture Radar (InSAR), the measured data is given as phase-valued or values on the one-dimensional sphere. When working with Electron Backscattered Diffractions Data (EBSD), the measured pixels are orientations, i.e. from the manifold $\mathrm{SO}(3)$ of all rotations or a quotient group of those due to symmetries in the observed crystal. Finally in Diffusion measurements such as Diffusion Tensor Magnetic Resonance Imaging (DT-MRI) the data items are given as symmetric positive definite matrices. All these applications have in common, that the values are given on a certain Riemannian manifold. Hence the obtained data is an image or even higher dimensional data structure that is manifold-valued.

Similar to classical images, the measurements of manifold-valued data might be obstructed by noise or some measurements be missing. Then, image processing methods have to be applied and classical methods therefrom to be adapted. For DT-MRI, several approaches exist, using tensor- or vector calculus with constraints or manifolds, see, e.g. [1, 2, 3]. One of the prominent mathematical fields in recent years is the variational approach, where the image processing task of interest is modeled as an energy functional to be minimized by developing efficient optimization methods.

Recently the TV regularization has been generalized to Riemannian manifolds [4, 5, 6, 7] and for the paper [6] the accompanying software is also available in the software package MFOPT[1]. They solve the variational problem by so-called lifting. On the other hand, for general optimization on manifolds have been developed, see [8, 9] for an overiew. The Manopt Toolbox[10][2] provides methods for the Newton iteration on manifolds including matrix completion problems and principle component analysis. They focus on a module approach, i.e. implementing the algorithms independently of the specific manifold at hand. These generic algorithms can then be applied using their manifolds or providing own ones.

In this paper we present the Manifold-valued Image Restoration Toolbox (MVIRT) [3] providing algorithms based on the proximal point algorithm and newton-type optimization algorithms for variational methods in manifold-valued image processing tasks. The toolbox also includes several algorithms and functions for handling the data at hand, especially visualization and exports. We also focus on a module based approach, i.e. the algorithms are implemented independently of the specific manifold at hand. The problems implemented in the manifold can also be seen as optimization problems with respect to Manopt, though the manifold-valued image requires then a product manifold the size of the number of pixels in their framework. We further focus on a the class of proximal point type algorithms, which also include the Douglas–Rachford splitting.

The remainder of the paper is organized as follows: We first introduce the mathematical definitions and models for variational methods on manifolds in Sect. 2. We then present three algorithms implemented within the MVIRT in Sec. 3. Finally we give an overview of the manifolds and algorithms implemented in the MVIRT and present a short example denoising diffusion tensors in Sect. 4

[1] see www.lellmann.net/work/soft ware/mfopt
[2] See manopt.org
[3] see www.mathematik.uni-kl.de/imagepro/members/bergmann/mvirt/

2. PRELIMINARIES

We first introduce the notations on Riemannian manifolds required for this proceedings paper and the general variational model we employ to formulate the image processing tasks in the following. For further details on manifolds we refer to [8, 11, 12].

2.1. Riemannian manifolds

Let $\mathcal{M}$ denote a complete n-dimensional Riemannian manifold, i.e. informally a set covered with a suitable collection of charts identifying subsets of $\mathcal{M}$ with $\mathbb{R}^n$, see e.g. [8]. We denote by $\langle\cdot,\cdot\rangle_x\colon \mathrm{T}_x\mathcal{M}\times\mathrm{T}_x\mathcal{M}\to\mathbb{R}$ the inner product in the tangential space $\mathrm{T}_x\mathcal{M}$ at $x\in\mathcal{M}$ and its induced norm by $\|\cdot\|_x$. Furthermore let $d_{\mathcal{M}}\colon \mathcal{M}\times\mathcal{M}\to\mathbb{R}$ denote the (geodesic) distance, i.e. the length of a shortest curve $\gamma_{\widehat{x,y}}\colon [0,d_{\mathcal{M}}(x,y)]\to\mathcal{M}$ called (minimizing) geodesic, connecting $x,y\in\mathcal{M}$. Note that the (minimizing) geodesic might not be unique. More general, the geodesics are those curves from x to y, along whose the covariant derivative of the vector field $\dot\gamma$ of the curve γ. For example on the two-dimensional sphere $\mathbb{S}^2 \coloneqq \{x\in\mathbb{R}^3 : \|x\|_2 = 1\}$ two points can be connected via great arcs, where both arcs from the great circle uniquely determined by x,y and the origin, if x,y are not antipodal. Both great arcs geodesics and the shorter one is the minimizing geodesic. For antipodal points, neither the great arc nor the arc being the minimizing curve in one great arc are unique. When not mentioned, we refer with the term geodesic to one of the minimizing geodesic.

Let $\gamma_{x,\xi}$, $x\in\mathcal{M}$, $\xi\in\mathrm{T}_x\mathcal{M}$, denote the unique geodesic with $\gamma_{x,\xi}(0) = x$ and $\dot\gamma_{x,\xi}(0) = \xi$. Finally we denote by $\exp_x\colon \mathrm{T}_x\mathcal{M}\to\mathcal{M}$, $\exp_x\xi \coloneqq \gamma_{x,\xi}(1)$ the exponential map and its local inverse, also called the logarithmic map by $\log_x = \exp_x^{-1}\colon \mathcal{M}\cap\mathcal{D}_x\to\mathrm{T}_x\mathcal{M}$, where D_x is the range where $\exp_x$ is bijective.

2.2. Variational model

In the following we introduce the variational model for the case of two-dimensional data. However, the generalization to higher dimensional data is straight forward and also available for the presented algorithm implementations. We denote by $\mathcal{G} \coloneqq \{1,\dots,N\}\times\{1,\dots,M\}$, $N,M\in\mathbb{N}$, the pixel grid of an N-by-M pixel image. In order to denoise or inpaint a manifold-valued image $f\colon\mathcal{G}\to\mathcal{M}$ we minimize functional of the form

$$\mathcal{E}(u) = \mathcal{E}(u;f) \coloneqq \mathcal{D}(u;f) + \mathcal{R}(u),$$

where the argument $u\colon\mathcal{G}\to\mathcal{M}$ is another manifold-valued image. In this formulation the first term $\mathcal{D}\colon\mathcal{M}\to\mathbb{R}$ denotes a similarity or data term and $\mathcal{R}\colon\mathcal{M}\to\mathbb{R}$ is the regularizer. For simplicity we denote one data item or pixel $f(p)$, $p\in\mathcal{G}$, in short by f_p. Furthermore $u^\star$ denotes a minimizer of $\mathcal{E}$, which is the result we aim for in the algorithms. Note that this minimization problem is high-dimensional and for the manifold-valued case often nonconvex.

In the following we focus on the data term

$$\mathcal{D}(u;f) \coloneqq \sum_{p\in\mathcal{G}} d^2_{\mathcal{M}}(f_p,u_p).$$

The Total variation (TV) formulation, cf. [13] for gray-valued TV, is one of the most used regularizers. It was generalized to the manifold-valued setting in [4, 5, 6, 7]

$$\mathcal{R}_{\mathrm{TV}}(u) \coloneqq \sum_{p\in\mathcal{M}}\sum_{q\in\mathcal{N}_p} d_{\mathcal{M}}(u_p,u_q)$$

where $\mathcal{N}_p \coloneqq \{(p_1+1,p_2)^{\mathrm{T}},(p_1,p_2+1)^{\mathrm{T}}\}\cap\mathcal{G}$ is the forward differences neighborhood. Then the TV regularization reads in variational formulation

$$\mathcal{E}_{\mathrm{TV}} \coloneqq \mathcal{D}(u;f) + \alpha\mathcal{R}_{\mathrm{TV}}(u),\quad \alpha>0. \tag{1}$$

For second order differences, we have to define a generalization of $\|x-2y+z\| = 2\|\frac{1}{2}(x+z)-y\|$ from Euclidean space. Denoting the mid points $\mathcal{C}_{x,z} \coloneqq c\in\mathcal{M} : \gamma_{\widehat{x,z}}(\frac{1}{2}d_{\mathcal{M}}(x,z))\}$, from all, i.e. not only the minimizing, geodesics $\gamma_{\widehat{x,z}}$, $x,z\in\mathcal{M}$, one can define the second order difference by the distance of y to the closest of the mid points of x and z, i.e.

$$d_2(x,y,z) \coloneqq \min_{c\in\mathcal{C}_{x,z}} d_{\mathcal{M}}(c,y),\qquad x,y,z\in\mathcal{M}.$$

Then the second order TV regularizer reads

$$\mathcal{R}_{\mathrm{TV}_2}(u) \coloneqq \sum_{p\in\mathcal{G}}\sum_{(q,r)\in\mathcal{N}'_p} d_2(q,p,r),$$

where

$$\mathcal{N}'_p \coloneqq \Big\{\big((p_1-1,p_2),(p_1+1,p_2)^{\mathrm{T}}\big), \big((p_1,p_2-1),(p_1,p_2+1)^{\mathrm{T}}\big)\Big\}\cap\mathcal{G}\times\mathcal{G}$$

denotes all sets of points, where p is the center point of the second order difference.

Then the second order variational model reads

$$\mathcal{E}_{\mathrm{TV}_2} \coloneqq \mathcal{D}(u;f)+\alpha\mathcal{R}_{\mathrm{TV}}(u)+\beta\mathcal{R}_{\mathrm{TV}_2}(u),\quad \alpha,\beta>0. \tag{2}$$

These models can be straightforwardly generalized to have different weights for horizontal and vertical differences and even include second oder mixed differences, see [14] for details.

In order to inpaint, let's assume we have a subset $\mathcal{V}\subset\mathcal{G}$ of the pixel grid given, where the data items f_p, $p\in\mathcal{V}$ are given but still might be obstructed by noise. Then the model for inpainting is given by modifying the data term to

$$\mathcal{D}_{\mathcal{V}}(u;f) \coloneqq \sum_{p\in\mathcal{V}} d^2_{\mathcal{M}}(f_p,u_p). \tag{3}$$

and the regularizer stays one from the above, such that the inpainted image $u^\star$ of the inpainting model is smooth.

3. ALGORITHMS

In the following we present three algorithms to compute the minimizer of one of the models from Subsec. 2.2. Note that a manifold-valued image can also be seen as $f \in \mathcal{M}^m$, where $m \coloneqq NM$ is the number of pixel. Note that $\mathcal{M}^m$ is also a Riemannian manifold with the usual product metric.

3.1. Cyclic proximal point algorithm

The proximal map was introduced on manifolds in [15] as

$$\operatorname{prox}_{\lambda\psi}(x) \coloneqq \arg\min_{y\in\mathcal{M}^m}\Big\{\frac{1}{2\lambda}\sum_{j=1}^{m} d^2_{\mathcal{M}}(x_j, y_j) + \psi(y)\Big\},$$

where $\lambda > 0$ and $\psi\colon \mathcal{M}^m \to \mathbb{R}\cup\{+\infty\}$. It was for example used in [16, 17] generalizing algorithms from the real line and vector space cases, see [18] for an overview.

Consider the additive decomposition of the variational functional $\mathcal{E} = \sum_{l=1}^{C}\varphi_l$ and a square summable but not summable sequence $\{\lambda_k\}_{k\in\mathbb{N}}$. Then the Cyclic Proximal Point Algorithm (CPPA) is given for a some initial $u^{(0)} \in \mathcal{M}^m$ as the iteration

$$u^{\left(k+\frac{l-1}{C}\right)} = \operatorname{prox}_{\lambda_k\varphi_l}\big(u^{(k+\frac{l-2}{C})}\big), \qquad l = 1,\dots,C, k = 1,2,\dots$$

until some convergence criterion is reached. In order for this algorithm to be fast, one needs a splitting of the involved variational functional into as few as possible summands and efficient implementations of the involved proximal maps. One can derive a splitting with $C = 5$ for the TV model (1) and to $C = 11$ for the first and second oder TV model (2), cf. [14].

For the involved proximal maps we have

- $\psi(x) = d_{\mathcal{M}}(x, f)$, $x \in \mathcal{M}$, given in closed form [15],
- $\psi(x, y) = d_{\mathcal{M}}(x, y)$, $(x, y) \in \mathcal{M}^2$, in closed form [7],
- $\psi(x, y, z) = d_2(x, y, z)$, $(x, y, z) \in \mathcal{M}^3$, given in closed form on $\mathcal{M} = \mathbb{S}^1$ in [19] and otherwise approximated, see [14].

The advantage is, that this algorithm is capable of handling the second order differences model, though due to its nonconvexity, the convergence is for now just observed numerically for a wider range of manifolds. For Hadamard manifolds, the first order algorithm converges. For other manifolds, convergence can be proven under mild conditions, see [19, 20]. A disadvantage is, that the CPPA is known to converge quite slowly in some cases.

3.2. Half-quadratic minimization

The Half-Quadratic Minimization Algorithm (HQMA) derived in [21] is not directly applied to the TV model (1) but to a relaxed model. The regularizer $\mathcal{R}_{\mathrm{TV}}$ is approximated by its relaxed version $\mathcal{R}_{\mathrm{TV},\varepsilon}$, $\varepsilon > 0$, where each distance term $d_{\mathcal{M}}(x, y)$ of neighboring pixel is replaced by $\mu(d_{\mathcal{M}}(x, y)), \mu(t) \coloneqq \sqrt{t^2 + \varepsilon^2}$. Finally one rewrites

$$\sqrt{d^2_{\mathcal{M}}(x, y) + \varepsilon^2} = ad^2(x, y) + \nu(a),$$

where $\nu(s) \coloneqq \min_{t\in\mathbb{R}}\{t^2 s - \varphi(t)\}$, $s \in \mathbb{R}$ is the c-transform of φ. Then the HQ algorithm consists of employing an alternating minimization over all pixel and all newly introduced variables a, where one variable is introduced for each first order difference in $\mathcal{R}_{\mathrm{TV}}$.

This algorithm can be computed by a Riemannian Newton method [8] for the manifold-valued part and a closed form solution exists for the minimization with respect to the introduced variables a. It converges on Hadamard manifolds and its convergence is observed to be faster than for the CPPA. A half-quadratic minimization algorithms for the second order difference TV model has still to be derived.

3.3. Douglas–Rachford splitting

The reflection operator of a function $\psi\colon \mathcal{M} \to \mathbb{R}\cup\{+\infty\}$ is given as

$$\mathcal{R}_\psi(x) = \exp_{\operatorname{prox}_\psi(x)}\big(-\log_{\operatorname{prox}_\psi(x)}(x)\big), \quad x \in \mathcal{M},$$

i.e. evaluating the geodesic from $\operatorname{prox}_\psi(x)$ to x at $t = -d_{\mathcal{M}}(x, \operatorname{prox}_\psi(x))$. Again for some splitting $\mathcal{E} = \sum_{l=1}^{C}\varphi_l$, we define $\Phi(\mathbf{x}) = \sum_{l=1}^{C}\varphi_l(x_l)$, $\mathbf{x} \in \mathcal{M}^{mC}$. In contrast to the CPPPA, the proximal map $\operatorname{prox}_{\lambda\Phi}$ can be evaluated by computing the proximal maps in parallel. Furthermore for the indicator function

$$\iota_D(\mathbf{x}) \coloneqq \begin{cases} 0, & \text{if } \mathbf{x} \in D,\\ \infty, & \text{else,}\end{cases}$$
$$D \coloneqq \{\mathbf{x} \in \mathcal{M}^{mC} : x_1 = \cdots = x_n \in \mathcal{M}^m\}$$

the proximal map $\operatorname{prox}_{\iota_D}$ is the projection onto D, i.e. for this set the Riemannian Center of Mass [22].

With these notations and fixed values $\lambda \in [0, 1], \eta > 0$, the Parallel Douglas Rachford Algorithm (PDRA) is given by iterating for $k = 1, 2, \dots$ the two computations

$$\mathbf{s}^{(k)} = \mathcal{R}_{\eta\Phi}\mathcal{R}_{\iota_D}\big(\mathbf{t}^{(k)}\big)$$
$$\mathbf{t}^{(k+1)} = \gamma_{\mathbf{t}^{(k)},\widehat{\mathbf{s}^{(k)}}}(\lambda)$$

for some starting value $\mathbf{t}^{(0)} \in \mathcal{M}^{mC}$, e.g. taking C copies of a starting value $u^{(0)} \in \mathcal{M}^m$.

While this algorithm converges on manifolds of nonpositive curvature [23] and numerically seems to converge as fast as the relaxed HQ minimization, it is ongoing research whether it works for general manifolds and how to incorporate higher order differences into the algorithm.

4. NUMERICAL EXAMPLES

The presented algorithms are implemented in the Manifold-valued Image Restoration Toolbox (MVIRT)[4]. It is implemented in Matlab using the object oriented features. Defininig your own manifold just requires to implement `exp`, `log`, `dist` and `addNoise` in order to already perform the TV regularization on a new manifold using the CPPA or the PDRA algorithm. All necessary functions like proximal maps, geodesics, or the Karcher mean are then available for the new manifold, too. The available algorithms are

CPPA An implementation of the CPPA for first and second order TV regularization from Subsec 3.1

HQMA The HQMA for TV regularization from Subsec. 3.2

DR The PDRA for TV regularization from Subsec. 3.3

median and mean following [24] and [25]

These algorithms are implemented in arbitrary-dimensional manifold-valued arrays, with optimized algorithms for the case of two-dimensional arrays, i.e. manifold-valued images. For the second order difference and its proximal map or the half-quadratic minimization a few more functions are required in order to enable the involved gradient descent algorithms, namely orthogonal bases of the tangential spaces and a parallel transport. The algorithms themselves are all implemented for an arbitrary manifold object. The following manifolds are available

Spheres n-dimensional spheres embedded in $\mathbb{R}^{n+1}$

Phase-values The circle can also be used with angles from $[0, 2\pi)$ instead of in the embedding in $\mathbb{R}^2$

Hyperbolic Spaces The n-dimensional hyperbolic manifold embedded in $\mathbb{R}^{n+1}$ including several isomorphisms, e.g. to the Poincaré half-plane and the Poincaré ball.

The Special Orthogonal Group The manifold of orientations represented by quaternions

Symmetric positive definite matrices The manifold of $n \times n$ symmetric positive definite matrices, including plot functions for the cases $n = 2, 3$ as ellipses and ellipsoids, respectively

Euclidean Space The Euclidean space, merely for reference

Their functions are mostly implemented in C/C++ using `mex` interfaces. They can be combined using the generic product manifold class.

To illustrate the toolbox we first start with an artificial example of a 16×16 pixel artificial image of symmetric positive definite matrices. They are visualized as ellipsoids in Fig. 1 (a), where each ellipsoid is colored using the geodesic anisotropy index from [26]. Loosing most of the data in (b) and obstructing the remaining part by Rician noise, $\sigma = 0.01$

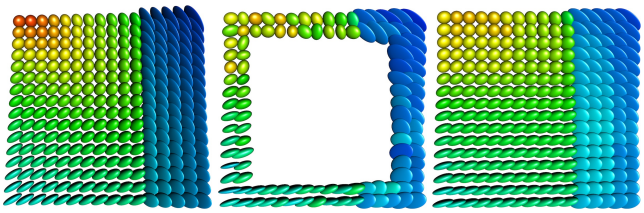

(a) Original data. (b) Lossy & noisy data, $\sigma = 0.01$ Rician. (c) Reconstruction $\alpha = 0.01$.

Fig. 1. Denoising and inpainting of artificial sym. pos. def. matrices $\mathcal{P}(3)$: The loss and obstruction by noise, see (b), of the original data from (a) can be reconstructed by model (1) using the PDRA (c), including the edge.

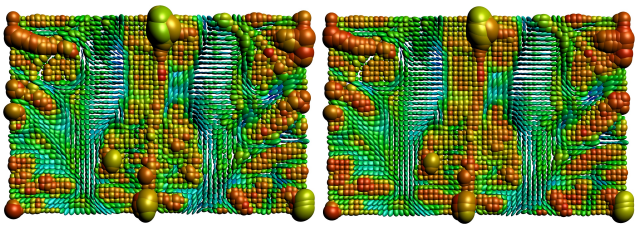

(a) Original slice. (b) TV denoised, $\alpha = 0.05$.

Fig. 2. Denoising a slice from the Camino dataset of DT-MRI data: (a) The original traversal slice 28 can be denoised using e.g. the Douglas-Rachford algorithm for the model (1).

the inpainting model, combining(3) into (1) and the Douglas-Rachford algorithm reconstruct the data, see Fig. 1 (c). The edge is inpainted as expected for a TV-type model and the complete image is denoised to a piecewise nearly-constant result. Applying the denoising to real data like a DT-MRI data from the Camino project[5][27] can denoise the measurement data, see Fig. 2.

Acknowledgement. The author wants to thank J. Persch and J. H. Fitschen for implementing parts of the Toolbox and discussing the implemented algorithms.

5. REFERENCES

[1] C.A. Castao-Moraga, C. Lenglet, R. Deriche, and J. Ruiz-Alzola, "A riemannian approach to anisotropic filtering of tensor fields," *Signal Processing*, vol. 87, no. 2, pp. 263–276, 2007.

[2] Zhizhou Wang, B. C. Vemuri, Y. Chen, and T. H. Mareci, "A constrained variational principle for direct estimation and smoothing of the diffusion tensor field from complex dwi," *IEEE Trans. Med. Imag.*, vol. 23, no. 8, pp. 930–939, 2004.

[3] C. Chefd'hotel, D. Tschumperlé, R. Deriche, and O. Faugeras, "Regularizing flows for constrained

[4] see www.mathematik.uni-kl.de/imagepro/members/bergmann/mvirt/

[5] see http://cmic.cs.ucl.ac.uk/camino

matrix-valued images," *J. Math. Imaging Vis.*, vol. 20, no. 1, pp. 147–162, 2004.

[4] E. Strekalovskiy and D. Cremers, "Total variation for cyclic structures: convex relaxation and efficient minimization," in *2011 IEEE Conference on Computer Vision and Pattern Recognition (CVPR)*. 2011, pp. 1905–1911, IEEE.

[5] E. Strekalovskiy and D. Cremers, "Total cyclic variation and generalizations," *Journal of Mathematical Imaging and Vision*, vol. 47, no. 3, pp. 258–277, 2013.

[6] J. Lellmann, E. Strekalovskiy, S. Koetter, and D. Cremers, "Total variation regularization for functions with values in a manifold," in *2013 IEEE International Conference on Computer Vision (ICCV)*, 2013, pp. 2944–2951.

[7] A. Weinmann, L. Demaret, and M. Storath, "Total variation regularization for manifold-valued data," *SIAM Journal on Imaging Sciences*, vol. 7, no. 4, pp. 2226–2257, 2014.

[8] P.-A. Absil, R. Mahony, and R. Sepulchre, *Optimization Algorithms on Matrix Manifolds*, Princeton and Oxford, Princeton University Press, 2008.

[9] M. Bačák, *Convex analysis and optimization in Hadamard spaces*, De Gruyter, Berlin, 2014.

[10] N. Boumal, B. Mishra, P.-A. Absil, and R. Sepulchre, "Manopt, a matlab toolbox for optimization on manifolds," *Journal of Machine Learning Research*, vol. 15, pp. 1455–1459, 2014.

[11] M. P. do Carmo, *Riemannian Geometry*, Birkhäuser, 1992.

[12] J. Jost, *Riemannian Geometry and Geometrix Analysis*, Springer-Verlang, Berlin Heidelberg, 2011.

[13] L. I. Rudin, S. Osher, and E. Fatemi, "Nonlinear total variation based noise removal algorithms," *Physica D: Nonlinear Phenomena*, vol. 60, no. 1, pp. 259–268, 1992.

[14] M. Bačák, R. Bergmann, G. Steidl, and A. Weinmann, "A second order non-smooth variational model for restoring manifold-valued images," *SIAM J. Sci. Comput.*, vol. 38, no. 1, pp. A567–A597, 2016.

[15] O. P. Ferreira and P. R. Oliveira, "Proximal point algorithm on Riemannian manifolds," *Optimization*, vol. 51, no. 2, pp. 257–270, 2002.

[16] M. Bačák, "The proximal point algorithm in metric spaces," *Israel Journal of Mathematics*, vol. 194, no. 2, pp. 689–701, 2013.

[17] M. Bačák, "Computing medians and means in Hadamard spaces," *SIAM Journal on Optimization*, vol. 24, no. 3, pp. 1542–1566, 2014.

[18] D. P. Bertsekas, "Incremental proximal methods for large scale convex optimization," *Mathematical Programming, Series B*, vol. 129, no. 2, pp. 163–195, 2011.

[19] R. Bergmann, F. Laus, G. Steidl, and A. Weinmann, "Second order differences of cyclic data and applications in variational denoising," *SIAM Journal on Imaging Sciences*, vol. 7, no. 4, pp. 2916–2953, 2014.

[20] R. Bergmann and A. Weinmann, "A second order tv-type approach for inpainting and denoising higher dimensional combined cyclic and vector space data," *Journal of Mathematical Imaging and Vision*, vol. 55, no. 3, pp. 401–427, 2016.

[21] R. Bergmann, R. H. Chan, R. Hielscher, J. Persch, and G. Steidl, "Restoration of manifold-valued images by half-quadratic minimization," *Inverse Problems in Imaging*, , no. 10, pp. 281–304, 2016.

[22] H. Karcher, "Riemannian center of mass and mollifier smoothing," *Communications on Pure and Applied Mathematics*, vol. 30, no. 5, pp. 509–541, 1977.

[23] R. Bergmann, J. Persch, and G. Steidl, "A parallel Douglas–Rachford algorithm for minimizing ROF-like functionals on images with values in symmetric Hadamard manifolds: extended version," *SIAM Journal on Imaging Sciences*, vol. 9, no. 4, pp. 901–937, 2016.

[24] R. Tron, B. Afsari, and R. Vidal, "On the convergence of gradient descent for finding the Riemannian center of mass," *SIAM Journal on Control and Optimization*, vol. 51, no. 3, pp. 2230–2260, 2013.

[25] P. T. Fletcher, S. Venkatasubramanian, and S. Joshi, "The geometric median on riemannian manifolds with application to robust atlas estimation," *NeuroImage*, vol. 45, no. 1 Supplement 1, pp. S143 – S152, 2009, Mathematics in Brain Imaging.

[26] M. Moakher and P. G Batchelor, "Symmetric positive-definite matrices: From geometry to applications and visualization," in *Visualization and Processing of Tensor Fields*, pp. 285–298. Springer Berlin Heidelberg, Berlin, Heidelberg, 2006.

[27] P. A. Cook, Y. Bai, S. Nedjati-Gilani, K. K. Seunarine, M. G. Hall, G. J. Parker, and D. C. Alexander, "Camino: Open-source diffusion-mri reconstruction and processing," in *Proc. Intl. Soc. Mag. Reson. Med. 14*, Seattle, WA, USA, 2006, p. 2759.